procedure of [7] was applied to alleviate the problems associated with the reactive discontinuities at section junctions. The couplers were constructed employing offset parallel-coupled striplines, with the line dimensions obtained from [9]. The tri-plate stripline structure consisted of two Duroid RT/5880 substrates of 31-mil thickness and relative permittivity 2.2, with a similar substrate of 5-mil thickness sandwiched between them. The transformers shown in Fig. 1(b) were implemented as 100–50-Ω impedance tapers, thereby matching the split to the 50-Ω coupler, and again to combine the two coupler output signals. Fig. 3 shows a photograph of the center substrate of the manufactured prototype, with the reference line on the left-hand side, and the phase shifter toward the right. The symmetrical phase shifter produced satisfactory results over a bandwidth of 1–17 GHz, as shown in Fig. 4. The results confirm the theory, but practical difficulties with especially the implementation of the splits were experienced. These were constructed using a number of via connections, and the resulting asymmetry deteriorated the high-frequency performance. Measured results for the reflection and transmission coefficients shown in Fig. 5 were also satisfactory. The insertion loss exceeds 3 dB at the higher end of the frequency range, but this may largely be attributed to inherent losses, as seen from the result shown for the reference line. Only a small portion of the curve for the reflection coefficient of the reference line is visible, since it is below -20 dB for nearly the whole frequency range.

A 90° phase shifter can be constructed by either cascading two 45° phase shifters, or by directly applying the synthesis technique. The latter will require a coupler with a nominal coupling coefficient of 0 dB, which may be realized by means of a tandem connection of two -3.01-dB couplers, or in practice, four -8.343-dB couplers. Employing couplers identical to those used in the previous example (i.e., $C_{0n} = -8.343$ dB and $\Delta C_n = 0.862$ dB) will result in a differential phase shift of $90° \pm 10°$. The insertion loss will ideally still be zero. However, due to the additional line length, the total dielectric and ohmic losses are expected to almost double in comparison to those of the 45° phase shifter. Applications where the input signal is to be simultaneously applied to both the input ports of a 90° phase shifter and the reference line will require the use of a power splitter. For these applications, a better option will be to merely use a symmetrical wideband -3.01-dB coupler as shown in Fig. 1(a), where a differential phase shift of 90° and negligible phase ripple between the signals at the coupled and through ports are established intrinsically.

IV. Conclusion

Progress in the field of wideband microwave has largely been limited to improvements or extensions to one of the six basic classes of Schiffman phase shifters, thereby restricting the realizability of these devices to about 9 : 1 bandwidth, up to 12 GHz. The novel class of ultrawideband phase shifters proposed here has the possibility of achieving up to a 20 : 1 bandwidth, extended to an upper limit of 20 GHz. Practical results confirmed the theory, although certain aspects like the implementation of the split to the coupler still need to be refined.

Acknowledgment

The authors acknowledge, with gratitude, the support of Grinaker Avitronics during the course of this research.

References

[1] B. M. Schiffman, "A new class of broad-band microwave 90° phase shifters," *IRE Trans. Microwave Theory Tech.*, vol. MTT-6, pp. 232–237, Apr. 1958.
[2] ——, "Multisection microwave phase shift network," *IEEE Trans. Microwave Theory Tech.*, vol. MTT-14, pp. 209, Apr. 1966.
[3] C. P. Tresselt, "Broad-band tapered-line phase shift networks," *IEEE Trans. Microwave Theory Tech.*, vol. MTT-16, pp. 51–52, Jan. 1968.
[4] V. P. Meschanov, I. V. Metelnikova, V. D. Tupikin, and G. G. Chumaevskaya, "A new structure of microwave differential phase shifter," *IEEE Trans. Microwave Theory Tech.*, vol. 42, pp. 762–765, May 1994.
[5] C. E. Free and C. S. Aitchison, "Improved analysis and design of coupled-line phase shifters," *IEEE Trans. Microwave Theory Tech.*, vol. 43, pp. 2126–2131, Sept. 1995.
[6] E. G. Crystal and L. Young, "Theory and tables of optimum symmetrical TEM-mode coupled-transmission-line directional couplers," *IEEE Trans. Microwave Theory Tech.*, vol. MTT-13, pp. 544–558, Sept. 1965.
[7] C. P. Tresselt, "The design and construction of broad-band high-directivity, 90° couplers using nonuniform line techniques," *IEEE Trans. Microwave Theory Tech.*, vol. MTT-14, pp. 647–656, Dec. 1966.
[8] J. A. G. Malherbe, *Microwave Transmission Line Couplers*. Norwood, MA: Artech House, 1988.
[9] J. P. Shelton, "Impedances of offset parallel-coupled strip transmission lines," *IEEE Trans. Microwave Theory Tech.*, vol. 14, pp. 7–15, Jan. 1966.

A Simple and Accurate MESFET Channel-Current Model Including Bias-Dependent Dispersion and Thermal Phenomena

Tae Moon Roh, Youngsik Kim, Youngsuk Suh, Wee Sang Park, and Bumman Kim

***Abstract*— A new channel-current model of GaAs MESFET suitable for applications to microwave computer-aided design (CAD) has been developed. This model includes the frequency-dispersion effects due to traps and thermal effects. The model parameters are extracted from pulsed *I–V* measurements at several ambient temperature and quiescent bias points. This model is verified by simulating nonlinear circuits, such as a power amplifier and a mixer.**

I. Introduction

For microwave-circuit design, commercially available computer-aided design (CAD) software is widely used. These CAD tools are based on the accurate device models, and a proper modeling is very important. In large-signal modeling, the gate–source and drain–source voltage-controlled drain–source channel current $I_{\rm ds}(v_{\rm gs}, v_{\rm ds})$ is the most important element because it is the major nonlinear component. The usual measurement method for determining $I_{\rm ds}(v_{\rm gs}, v_{\rm ds})$ is pulsed *I–V* technique [1]-[5], which is free from the frequency dispersion due to deep-level trap/surface state and thermal

Manuscript received November 5, 1996; revised April 25, 1997. This work was supported in part by the Agency for Defense Development.

T. M. Roh, Y. Kim, W. S. Park, and B. Kim are with the Department of Electronic and Electrical Engineering and Microwave Application Research Center, Pohang University of Science and Technology, Pohang, Kyung-pook, 790-784, Korea.

Y. Suh is with the School of Electrical and Electronic Engineering Yeungnam University, Gyongsan, Kyungbuk, 712-749, Korea.

Publisher Item Identifier S 0018-9480(97)05383-0.

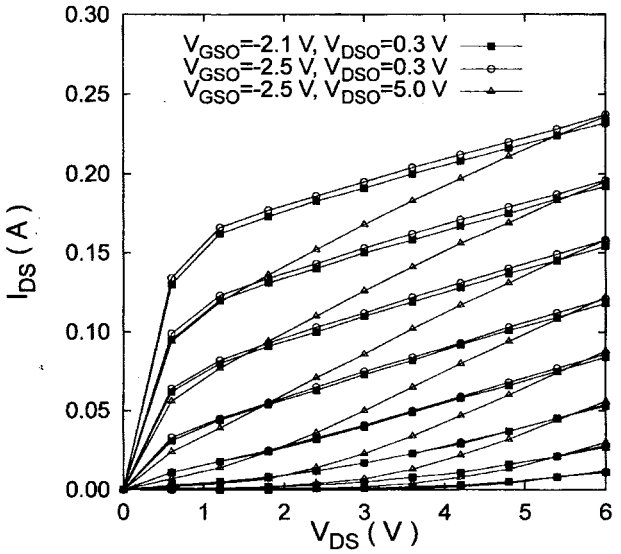

Fig. 1. Comparison of experimental pulsed *I–V* data (OKI KGF-1284 GaAs MESFET, $V_{\rm gmin} = -2.6$ V, $V_{\rm gmax} = -1.55$ V, step $= 0.15$ V).

effects due to the internal power dissipation [6]–[8]. However, the dynamic *I–V* data from the pulsed measurements are strongly dependent on the quiescent bias conditions. An accurate drain-current model should be capable of predicting the dynamic current behavior for different quiescent bias conditions ($V_{\rm gso}$, $V_{\rm dso}$). The dynamic channel currents can be modeled using the first-order function of gate and drain quiescent voltages; $I_{\rm ds}(v_{\rm gs}, v_{\rm ds}, V_{\rm gso}, V_{\rm dso})$[4].

In this investigation, a new simple bias-dependent channel-current model is presented. This model represents all required characteristics, i.e., frequency-dispersion effects, thermal phenomena, and higher order derivative terms of $I_{\rm ds}$, which are important for predicting harmonic components [9]–[11]. The authors' model is applied to the design of a power amplifier and mixer, and its simulation capability is experimentally verified.

II. New Channel-Current Model Including Bias-dependency and Thermal Phenomena

For the modeling of the dynamic channel-current $I_{\rm ds}(v_{\rm gs}, v_{\rm ds}, V_{\rm gso}, V_{\rm dso})$, pulsed *I–V* measurements should be performed at the several quiescent bias conditions ($V_{\rm gso}$, $V_{\rm dso}$) due to the trapping effect [1]–[5]. According to Filicori's results [4], only a weak correlation exists between the gate quiescent bias and the drain quiescent bias effect. Therefore, $I_{\rm ds}$ can be modeled as a separated first-order function of $V_{\rm gso}$ and $V_{\rm dso}$. The *I–V* curve of OKI KGF-1284 GaAs MESFET's is measured at several bias points (shown in Fig. 1). This figure is obtained from measurements at three different bias conditions with low $V_{\rm gso}$ and low $V_{\rm dso}$, low $V_{\rm gso}$ and high $V_{\rm dso}$, and high $V_{\rm gso}$ and low $V_{\rm dso}$. All of these biases lead to different states of the traps with negligible power dissipation. As the drain quiescent bias voltage increases, the dynamic output conductance increases and the channel-current decreases. The gate quiescent bias variation changes the magnitude of channel current a little. These drain and gate quiescent bias effects are similar to the previously reported results [2], [4], [5].

Another important issue of channel-current modeling is the capability of representing temperature effects and higher order derivatives of transconductance. Based on Pedro's channel-current model [11], an improved channel-current model is proposed as follows:

$$
\begin{aligned}
I_{\rm dsRF} &= \beta[u + \log(e^{u} + e^{-u})]\tanh(\alpha v_{\rm ds}) \\
V_p &= V_{po} + \gamma v_{\rm ds}, \qquad d = \left(\frac{v_b - v_{\rm gs}}{V_p}\right) \\
u &= A(1-d) - C \qquad (1) \\
v_b &= v_{bo} + v_{b,dso} * V_{\rm dso} \\
A &= A_o + A_{\rm dso} * V_{\rm dso} \\
\beta &= \beta_o + \beta_{\rm gso} * V_{\rm gso} + \beta_T * \Delta T_j \\
\gamma &= \gamma_o + \gamma_{\rm dso} * V_{\rm dso} + \gamma_T * \Delta T_j \\
\alpha &= \alpha_o + \alpha_{\rm dso} * V_{\rm dso} + \alpha_{\rm gso} * V_{\rm gso} \\
\Delta T_j &= R_\theta\,[(1-\eta)P_o - P_o^*] + (T_a - T_a^*) \qquad (2)
\end{aligned}
$$

where d represents the depletion width. u, which is a function of d, A, and C can be interpreted as the active channel height. The parameters v_b, A, β, γ, and α are represented by quiescent bias points and temperatures. The channel temperature difference is ΔT_j, power-added efficiency η, thermal resistance $R_{\rm th}$, dc input power, and ambient temperature of the device P_o and T_a at the operation condition, dc input power and ambient temperature of the device P_o^* and T_a^* in modeling procedure, respectively. The pinchoff voltage V_p is $V_{\rm ds}$ dependent in order to represent the observed turn-on voltage variation with drain bias and to improve the output conductance description. Representing *I–V* curve variations due to the quiescent bias ($V_{\rm dso}$, $V_{\rm gso}$), and channel temperature (ΔT_j), the parameters in (2) are expressed as the first-order functions of $V_{\rm dso}$, $V_{\rm gso}$, and ΔT_j. For predicting drain quiescent bias effects, the parameters $v_{b,dso}, \alpha_{\rm dso}, \gamma_{\rm dso}$, and $A_{\rm dso}$ are expressed as functions of $V_{\rm dso}$. The gate quiescent bias effect can be predicted by the parameters $\beta_{\rm gso}$, and $\alpha_{\rm gso}$. The channel pinchoff voltage and transconductance are affected by the channel temperature and the effect is accounted for by the parameters γ_T and β_T. The internal power dissipation of the transistor in the modeling (pulsed measurement at quiescent bias point) is different from the real RF-operation due to the dc to RF conversion efficiency (η). This effect is considered by introducing η.

III. Modeling and Experimental Result

In order to validate this paper's channel-current equation, a nonlinear model has been extracted for OKI KGF-1284 MESFET. Using the optimization method, the parameters V_{po}, v_b, A, C, β, γ, and α in (1) are extracted from the pulsed *I–V* data at a quiescent bias point and an ambient temperature. The extracted parameters from the measured pulsed *I–V* data at different temperatures with a bias point $V_{\rm gso} = -2.2$ V and $V_{\rm dso} = 3$ V are shown in Table I. The temperature effect terms in γ and β, represented by parameters γ_T and β_T, are calculated from Table I. The extracted γ_T's and β_T's under the different quiescent bias points show similar values. From the pulsed *I–V* data for several quiescent biases with the same ambient temperature and internal-power dissipation, the seven parameters in (1) are extracted. The gate quiescent bias dependency parameters ($\beta_{\rm gso}, \alpha_{\rm gso}$) and drain quiescent bias dependency parameters ($v_{b,\rm dso}, \alpha_{\rm dso}$, $A_{\rm dso}, \gamma_{\rm dso}$) are calculated from the parameters following the same procedure in the temperature-dependent parameter extraction. Complete channel-current model parameters are shown in Table II. Also, the nonlinear capacitors and linear elements in the large-signal model are extracted from the bias dependent S-parameters [12], [13]. The extracted complete large-signal model with channel-current equation and other parameters has been implemented using the symbolic defined-device model (SDD) in HP-EEsof MDS. Fig. 2 compares the pulsed measurements with the model. The model

TABLE I
PARAMETERS OF THE CHANNEL-CURRENT MODEL FOR OKI KGF-1284 ($V_{gso} = -2.2$ V, $V_{dso} = 3$ V)

	Bias Condition (V_{gso} = -2.2 V, V_{dso} = 3 V)		
	T_a^* = 25 ℃, ΔT_j = 3 ℃	T_a^* = 45 ℃, ΔT_j = 23 ℃	T_a^* = 65 ℃, ΔT_j = 43 ℃
V_{po}	-1.3565		
v_b	0.1979		
A	18.2723		
C	-2.3326		
β	0.025026	0.025250	0.0254762
γ	-0.080289	-0.078086	-0.075887
α	2.1533		

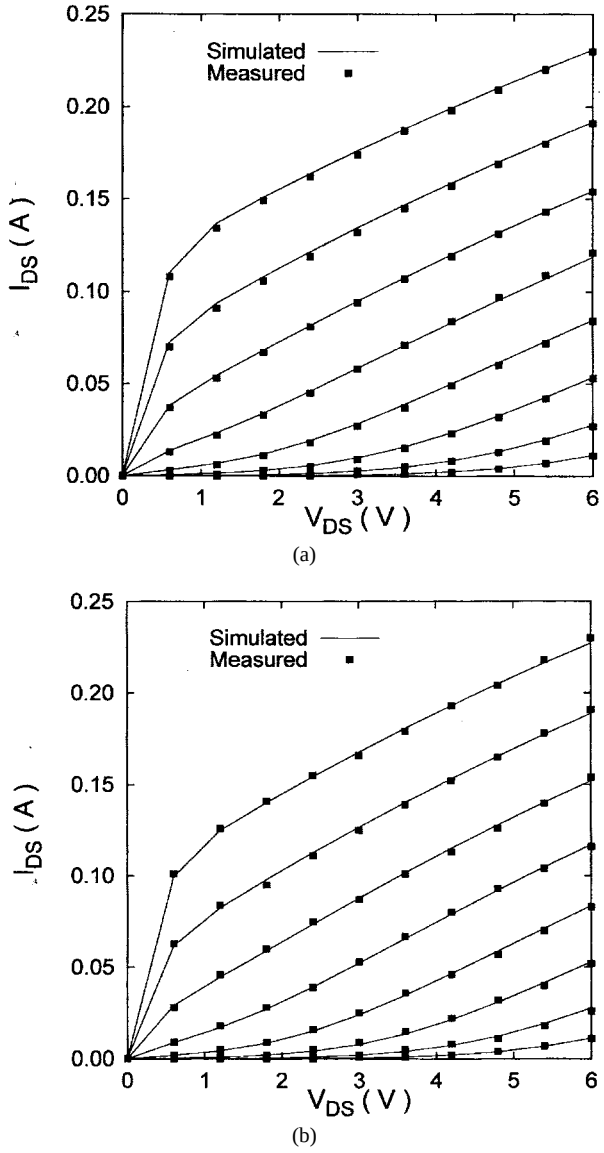

Fig. 2. Measured and simulated pulsed *I–V* curves ($V_{gmin} = -2.6$ V, $V_{gmax} = -1.55$ V, step = 0.15 V) (a) quiescent point: $V_{gso} = -2.2$ V, $V_{dso} = 3$ V (b) quiescent point: $V_{gso} = -2.0$ V, $V_{dso} = 4$ V.

is capable of reproducing the variations in *I–V* curve with the quiescent point very well. Fig. 3 shows the agreement between the

TABLE II
PARAMETERS OF THE COMPLETE CHANNEL-CURRENT MODEL FOR OKI KGF-1284 (INCLUDING BIAS AND THERMAL EFFECTS)

V_{po}	-1.3565
v_b	v_{bo} : 0.3344, $v_{b,dso}$: -0.045527
A	A_o : 17.226, A_{dso} : 0.34834
C	-2.3326
β	β_o : 0.023177, β_{gso} : -8.25e-4, β_T : 1.125e-5
γ	γ_o : -0.05815 , γ_{dso} : 0.00749, γ_T : 1.101e-4
α	α_o : 0.28499, α_{dso} : 0.11704, α_{gso} : -0.6721

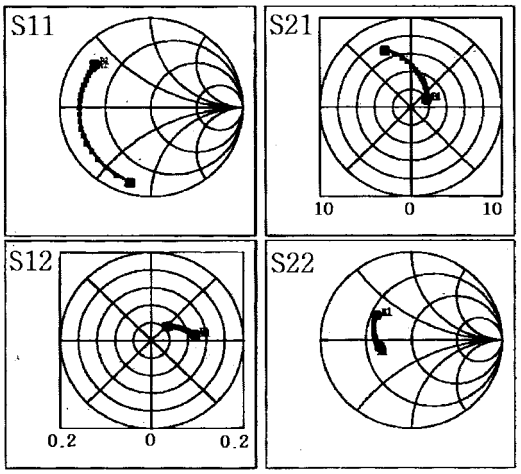

Fig. 3. Measured and simulated S-parameter using large-signal model (points: measured, lines: simulated) (OKI KGF-1284, $V_{gso} = -2.0$ V, $V_{dso} = 4$ V, frequency: 0.6–3 GHz).

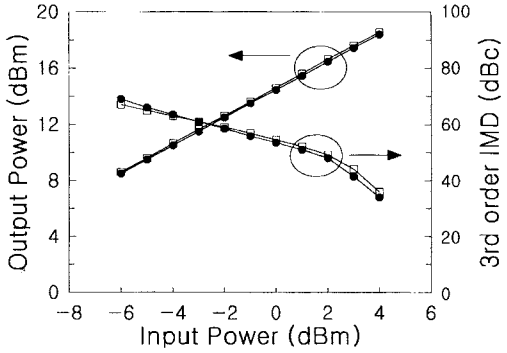

Fig. 4. Comparison of experimental (□) and simulated (•) results for power amplifier performance.

measured small-signal S-parameters and simulation results using this paper's large-signal model in the frequency band from 0.6 to 3 GHz. The transconductance and output resistance extracted from the S-parameter are 0.234 S, 42.2 Ω, and the same parameters extracted from the *I–V* curve are 0.231 S, 44.3 Ω at $V_{gso} = -2.0$ V, $V_{dso} = 4$ V. These data confirm that the proposed model is very accurate.

A one-stage power amplifier has been fabricated with these MESFET's. Fig. 4 shows measured and simulation results of the two-tone output power and IMD_3 for the input-power sweep from −6 to 4 dBm. At the frequency of 1750 MHz and $V_{dso} = 4.2$ V, the maximum differences of IMD_3 and output power are 2 dB and 0.2 dBm, respectively. Using the same methodology, a 400-μm-wide

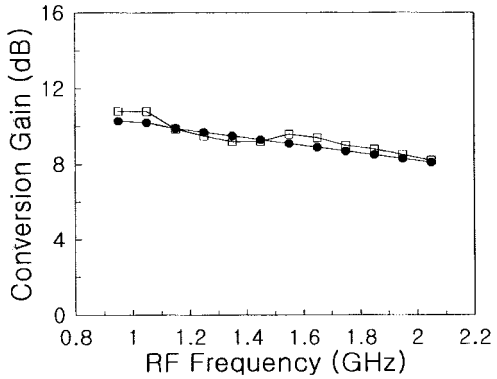

Fig. 5. Comparison of experimental (□) and simulated (•) results for MMIC mixer performance.

MESFET from Kukje has been modeled and a monolithic-microwave-integrated-circuit (MMIC) mixer has been designed and tested for PCS applications. Fig. 5 shows the measured and simulation results of the conversion gain for the frequency range from 0.95 to 2.05 GHz. The maximum conversion-gain difference is less than 1 dB.

IV. Conclusion

In this paper, a very simple new-channel-current model has been proposed, which can represent the frequency-dispersion effects due to traps, channel temperature effect, and higher order derivative terms of $I_{\rm ds}$. The derivative terms are important for predicting nonlinear circuit performance. The model parameters are extracted from the pulsed *I–V* measurements at several ambient temperatures and quiescent bias points. The extraction procedure is straightforward and simple. In order to validate this model, a large-signal model has been extracted for OKI KGF-1284 and Kukje MESFET. The extracted large-signal MESFET models have been implemented using SDD in HP-EEsof MDS. By comparing the pulsed *I–V* and S-parameter measurements with simulation results, the accuracy of this model was verified. This model has also been applied to the design of nonlinear circuits such as power amplifiers and mixers. The harmonic-balance simulations with the proposed model and the experimental results for fabricated circuits confirm the accuracy of the proposed modeling.

References

[1] M. Paggi, P. H. Williams, and J. M. Borrego, "Nonlinear GaAs MESFET modeling using pulsed gate measurements," *IEEE Trans. Microwave Theory Tech.*, vol. 36, pp. 1593–1597, Dec. 1988.

[2] T. Fernandez, Y. Newport, J. M. Zamanillo, A. Tazon, and A. Mediavilla, "Modeling of operating point nonlinear dependence of Ids characteristics from pulsed measurements in MESFET transistors," in *23rd European Microwave Conf. Dig.*, Madrid, Spain, Sept. 1993, pp. 518–521.

[3] F. Filicori, G. Vanni, A. Mediavilla, and A. Tazon, "Modeling of deviations between static and dynamic drain characteristics in GaAs FET's," in *23rd European Microwave Conf. Dig.*, Madrid, Spain, Sept. 1993, pp. 454–457.

[4] F. Filicori, G. Vanni, A. Santarelli, A. Mediavilla, A. Tazon, and Y. Newport, "Empirical modeling of low-frequency dispersive effects due to traps and thermal phenomena in III-V FET's," *IEEE Trans. Microwave Theory Tech.*, vol. 43, pp. 2972–2981, Dec. 1995.

[5] T. Fernandez, Y. Newport, J. M. Zamanillo, A. Tazon, and A. Mediavilla, "Extracting a bias-dependent large signal MESFET model from pulsed *I/V* measurements," *IEEE Trans. Microwave Theory Tech.*, vol. 44, pp. 372–378, Mar. 1996.

[6] P. H. Ladbrooke and S. R. Blight, "Low-field low-frequency dispersion of transconductance in GaAs MESFET's with implications for other rate-dependent anomalies," *IEEE Trans. Electron Devices*, vol. 35, pp. 257–267, 1988.

[7] J. A. Reynoso-Hernandez and J. Graffeuil, "Output conductance frequency dispersion and low-frequency noise in HEMT's and MESFET's," *IEEE Trans. Microwave Theory Tech.*, vol. 37, pp. 1478–1481, Sept. 1989.

[8] J. M. Golio, M. G. Miller, G. N. Maracas, and D. A. Johnson, "Frequency-dependent electrical characteristics of GaAs MESFET's," *IEEE Trans. Electron Devices*, vol. 37, pp. 1217–1227, May 1990.

[9] S. A. Mass and D. Neilson, "Modeling MESFET's for Intermodulation Analysis of Mixers and Amplifiers," *IEEE Trans. Microwave Theory Tech.*, vol. 38, pp. 1964–1971, Dec. 1990.

[10] ____, "Modeling GaAs MESFET's for intermodulation analysis," *Microwave J.*, pp. 295–300, May 1991.

[11] J. C. Pedro and J. Perez, "A novel non-linear GaAs FET model for intermodulation analysis in general purpose harmonic-balance simulators," in *23rd European Microwave Conf. Dig.*, Madrid, Spain, Sept. 1993, pp. 714–716.

[12] W. R. Curtice, "GaAs MESFET modeling and nonlinear CAD," *IEEE Trans. Microwave Theory Tech.*, vol. 36, pp. 220–230, Feb. 1988.

[13] J. Rodriguez-Tellez, K. A. Mezher, O. M. Conde Portilla, and J. C. Luengo Patrocinio, "A highly accurate microwave nonlinear MESFET model," *Microwave J.*, pp. 280–285, May 1993.

Two-Port Scattering at an Elliptic-Waveguide Junction

Kin-Lung Chan and Sunil R. Judah

***Abstract*— A concentric waveguide junction consisting of an elliptic waveguide has been formulated using the mode-matching method. The formulation is a generalized solution of the problem such that the second waveguide, which forms the junction, can be any regular shape in cross section. Exact closed-form expressions for computing the coupling integrals have been obtained from the generalized formulation. As a special case of the general solution, the expressions for evaluating the coupling integrals of rectangular-to-elliptic, circular-to-elliptic, and elliptic-to-elliptic waveguide junction are given. Theoretical results compare well with the experimental and published results.**

***Index Terms*—Elliptic waveguide, mode-matching method, waveguide junction.**

I. Introduction

One of the advantages of using elliptic waveguides is that the spectral separation between propagating modes can be varied by changing the eccentricity. It then prevents mode coupling due to imperfection of waveguide curvature or waveguide bending, as happens in a circular waveguide. The desired propagating mode, therefore, can be preserved. The use of elliptic waveguides is becoming more popular in microwave systems and the behavior of transition from waveguides having different geometries to elliptic waveguides becomes important.

The formulations of waveguide discontinuities involving rectangular or circular waveguides have been well documented in the literature [1]–[5]. Recently, Matras *et al*. [6] studied the scattering

Manuscript received June 13, 1996; revised March 17, 1997.

The authors are with the Department of Electronic Engineering, University of Hull, Hull, HU6 7RX U.K.

Publisher Item Identifier S 0018-9480(97)05384-2.